Unveiling the anti-inflammatory effect of *Perilla frutescens* essential oil by using multi-omics analysis in zebrafish model

Yao Fu[1,2], Jie Cheng[1,2], Xianghe Meng[2,3], Guicai Tang[4], Li Li[5,6], Ziyoviddin Yusupov[7], Komiljon Tojibaev[7], Min He[1,2]*, Mengmeng Sun[1,2]*

[1]Changchun University of Chinese Medicine, Jingyue Economic Development District, Changchun, China; [2]The Jilin Province School-Enterprise Cooperation Technology Innovation Laboratory of Herbal Efficacy Evaluation Based on Zebrafish Model Organisms, Changchun University of Chinese Medicine, Jingyue Economic Development District, Changchun, China; [3]Wish Technology, Beihu Science and Technology Park, High-Tech North District, Changchun, China; [4]Baishan Institute of Science and Technology, Hunjiang District, Baishan, China; [5]Beijing Institute of Traditional Chinese Medicine, Shuiche Alley Xinjiekou, Xicheng District, Beijing, China; [6]Capital Medical University, Subsidiary Beijing Hospital of Traditional Chinese Medicine, Dongcheng District, Beijing, China; [7]Institute of Botany, Academy of Sciences of Uzbekistan, Tashkent, Uzbekistan

***Corresponding Authors:** Min He (Email: hemin@ccucm.edu.cn) and Mengmeng Sun (Email: sunmm@ccucm.edu.cn), Changchun University of Chinese Medicine, No. 1035, Boshuo Rd, Jingyue Economic Development District, Changchun 130117, China

Academic Editor: Teresa D'Amore, PhD, Laboratory of Preclinical and Translational Research, IRCCS CROB, Centro di Riferimento Oncologico della Basilicata, 85028 Rionero in Vulture, Italy

Received: 13 November 2024; Accepted: 27 March 2025; Published: 1 July 2025

RESEARCH ARTICLE

Abstract

Perilla frutescens essential oil (PFO) is a mixture of volatile compounds extracted from the aboveground part of *Perilla frutescens* (L.) Britt. Besides its pleasant aroma, PFO exhibits many biological activities, which have significant promise for the creation of functional foods. The present study aimed to reveal the anti-inflammatory effect of PFO in zebrafish tail fin amputation model by observing neutrophil migration. Our results showed that perilla ketone (42.41%) is the main component of PFO, and 3.0 μg/mL of PFO significantly inhibited neutrophils migration to the amputation site. In addition, PFO had the noticeably regulatory effect on the expression of tumor necrosis factor α, interleukin 6, and interleukin 1β. Multi-omics analysis identified two crucial genes (peptide YYa [*pyya*] and *glula*) and 20 significant metabolites affected by PFO, revealing that PFO intervenes in inflammatory response by regulating arginine biosynthesis, alanine, aspartate, and glutamate metabolism, glyoxylate and dicarboxylate metabolism, and neuroactive ligand–receptor interaction. Subsequent study showed that *pyya* and *glula* sequentially connected these metabolic pathways, and PFO could control the expression of these two crucial genes ($P < 0.0001$). These results serve as a significant reference for PFO's worth in development and sensible utilization as a safe, healthy, and natural functional food in the future.

Keywords: anti-inflammatory effect; essential oil; multi-omics; *Perilla frutescens*; zebrafish model

Introduction

Perilla frutescens (L.) Britt., an aromatic herbaceous plant classified in the Lamiaceae family, is a native to several Asian countries, such as China, Japan, Korea, and Vietnam. Often known as *Zisu* in China, it has been cultivated as a significant medicinal plant for more than two millennia (Wu *et al.*, 2023). *Perilla frutescens* leaves are frequently utilized as a healthy culinary herb and flavor enhancer because of their fragrant flavor. The oil extracted from the seeds of *Perilla frutescens* is often consumed as a nutritive cooking oil in Mainland China (Huang *et al.*, 2011). In addition to its culinary use, *Perilla frutescens* has attracted considerable attention as a traditional Chinese medicine for treating ailments such as cold, cough, and headaches (Ji *et al.*, 2014; Yu *et al.*, 2017). Extensive research has been conducted on the leaf, stem, and seed of *Perilla frutescens*. These studies have demonstrated that these parts of the plant possess antioxidant (Masuda *et al.*, 2018), anti-inflammatory (Chen *et al.*, 2015), antibacterial (Ghimire *et al.*, 2017), antifungal (Tian *et al.*, 2014), anti-allergic (Makino *et al.*, 2003), anticancer (Reddy *et al.*, 2021), and antidepressant (Zhong *et al.*, 2024) properties. The pharmacological benefits of *Perilla frutescens* are ascribed to its plentiful bioactive constituents, such as flavonoids, essential oil, unsaturated fatty acids, triterpenes, and phenolic compounds (Yu *et al.*, 2017).

Essential oil, an intricate blend of secondary metabolites (Pavela and Benelli, 2016), is synthesized and secreted by aromatic and spices plants. The unique aroma of *Perilla frutescens* leaves is attributed to the essential oil constituents present in the glandular trichomes located on the underside of leaves (Zhou *et al.*, 2021). Essential oil derived from *Perilla frutescens* (PFO) is granted the 'generally recognized as safe status' for use as a food flavoring substance in China (Li *et al.*, 2018). It is suitable for incorporation in various food items, such as baked goods, drinks, frozen dairy products, and pudding (Li *et al.*, 2018). In addition, current research predominantly focuses on the bioactive effect of PFO regarding its antidepressive (Nguyen *et al.*, 2024b), antihyperlipidemic (Omari-Siaw *et al.*, 2016), and antibacterial characteristics (Ahmed and Al-Zubaidy, 2020), and inhibits the expression of relevant pro-inflammatory cytokines at cellular level (Wang *et al.*, 2018; Zi *et al.*, 2021). Additional investigation is required to fully understand the anti-inflammatory mechanism of PFO *in vivo*.

Inflammation serves as the fundamental cause of several physiological and pathological processes. It is initiated by several harmful situations, such as infection and tissue damage. The incidence and prevalence of common inflammatory illnesses, such as inflammatory bowel disease (IBD), have risen significantly globally, with prevalence proportion exceeding 0.3% in Western countries, thus presenting a considerable public health challenge (Ng *et al.*, 2017). The paradigmatic catalysts of inflammatory process are acknowledged for their role in driving the migration of leukocytes and plasma proteins to the site of injured tissue (Wang, 2018). Neutrophils are the initial cells recruited and dispatched to the injured tissue, where they contribute to the stimulation of inflammatory response (Campos-Sánchez and Esteban, 2021; Margraf *et al.*, 2019). Inflammation is a complex interaction of immunological, physiological, and behavioral processes that involves a wide range of signaling pathways. Various cell types synthesize inflammatory cytokines, such as tumor necrosis factor-α (TNF-α), Interleukin 1β (IL-1β), and Interleukin 6 (IL-6), etc. Their functioning in inflammatory response involves several actions, including stimulating the activation of the endothelium and leukocytes as well as beginning the acute-phase response (Chopra *et al.*, 2024). Once the inflammation diminishes, the body reestablishes its condition of homeostasis.

The zebrafish is widely used as an animal model in biomedical research because of its significant advantages, such as its high genetic resemblance to humans, rapid developing timeline, transparent embryos, and low-dose requirements of tested drugs. The transgenic zebrafish demonstrates genetic stability and is very suitable for microscopic imaging of cellular activity during the phases of development and diseases, including both embryonic and larval stages (Choe *et al.*, 2021).

The tail fin amputation model in larval zebrafish is a well-established method for evaluating the effectiveness of anti-inflammatory agents (He *et al.*, 2020; Zanandrea *et al.*, 2020). The tail fins of larvae, 3 days post-fertilization (dpf), were removed surgically. Afterwards, neutrophils, which are the most abundant type of white blood cells (WBCs) at this stage of development, moved toward the injured location. To track the movement of neutrophils, the zebrafish strain commonly used in this assay is *Tg* (mpx: GFP), wherein the myeloid-specific peroxidase (mpx) was genetically engineered to express green fluorescent protein (GFP). The quantity of migrating neutrophils is regarded as an indicator of the intensity of inflammatory reaction (Speirs *et al.*, 2024). The zebrafish model is widely applied in many essential oils to investigate toxicity, safety, and bioactivity (Wang *et al.*, 2023). As far as we know, this *in vivo* model has not been utilized yet to study the anti-inflammatory properties of PFO.

The present study, aimed to analyze the chemical composition of PFO, investigated the application of anti-inflammatory activity in transgenic larval zebrafish (*Tg* (mpx:GFP)) tail fin amputation model, and reveal the anti-inflammatory effect of PFO by a combination of

transcriptomics and metabolomics analysis. Multi-omics denotes the utilization of two or more omics methodologies (e.g., transcriptomics, metabolomics, etc.) to examine genes, metabolites, biomarkers, and other elements that substantially influence a study. For instance, by combining transcriptomics and metabolomics analyses, researchers identified PLA2G2A as a significant biomarker and crucial therapeutic target for lipid metabolism-associated genes in ulcerative colitis (Ding *et al.*, 2024). Hence, our discoveries enhance the comprehension of the anti-inflammatory process of PFO and offer fresh empirical proof for using PFO in anti-inflammatory functional foods.

Materials and Methods

Chemicals and reagents

Perilla frutescens were harvested from Baishan city, Jilin Province in China. The plants were initially identified using morphological features and then confirmed by Prof. Mengmeng Sun at Changchun University of Chinese Medicine. The steam distillation method was used to extract essential oil from the leaves of *Perilla frutescens*. Tween-80 was acquired from Beijing Solarbio Science & Technology Co. Ltd. (China). Beclomethasone and tricaine were purchased from Shanghai Yuanye Bio-Technology Co. Ltd. (China). All organic reagents (ethyl acetate, trichloromethane isopropanol, etc.) were acquired from Sigma-Aldrich (USA). The purity of all chemicals substances exceeded 98%.

Gas chromatography–mass spectrometry (GC-MS) analysis

Agilent8890 gas chromatography and Agilent7700D mass spectrometer (Agilent Technologies Inc., USA) were used to separate and identify the essential oil sample, respectively. Agilent HP-5 MS column (30m×0.25 mm, 0.25 μm) with 5% phenyl methyl siloxane was equipped with gas chromatography, while an electrospray ionization interface was used as an ion source for mass spectrometry (Liu *et al.*, 2013). Detection conditions are listed in Appendix 1. Subsequently, qualitative analysis was conducted using the Mass Hunter software. Component identification involved matching their recorded mass spectra with standard mass spectra obtained from the National Institute of Standards and Technology (NIST20) libraries provided by the GC-MS system software as well as referencing literature data and standards of the main components. For quantitative analysis, the area percentage of each component of essential oil was determined through peak area normalization measurement.

Zebrafish Lines and Maintenance

According to the standards of the Zebrafish Model Organism Database (http://zfin.org), the zebrafish used in this study were well cared for and managed, and completely complied with the regulations of the Local Animal Welfare Council of Changchun University of Chinese Medicine. To maintain circadian rhythmicity, they were exposed to a 14-h light and 10-h dark cycle (He *et al.*, 2020). Two healthy pairs of male and female zebrafish, aged 6–12 months, were selected at the onset of light to naturally induce fertilization. The eggs were collected and cultivated at a temperature of 28°C in egg water consisting of 60 μg/mL Instant Ocean sea salts and 0.0025% methylene blue. In addition to wild type zebrafish (AB), a transgenic line (*Tg* (mpx:GFP)) was also employed in this study for establishing a tail-fin amputation model and investigating neutrophil migration patterns. All animal procedures strictly adhered to the Guidelines for Care and Use of Laboratory Animals set forth by Changchun University of Chinese Medicine. The experiments received proper authorization from the Animal Ethics Committee of Changchun University of Chinese Medicine (No. 2022454).

Toxicity test for PFO

Tween-80 was used as a co-solvent (Lin *et al.*, 2016) to dissolve PFO in egg water to prepare solutions with concentrations of 0.3 μg/mL, 0.6 μg/mL, and 3.0 μg/mL. The safe concentration of Tween-80 was also evaluated experimentally. Zebrafish larvae, 3-day-old, were exposed to a solution of egg water with different concentrations of PFO/Tween-80 for 96 h. During this time frame, the researchers systematically observed the fatal and teratogenic effects of PFO/Tween-80 on zebrafish at intervals of 24 h, 48 h, 72 h, and 96 h.

Tail fin amputation and drug treatments

The tail fin amputation experiments were conducted using 3-day-old larvae, and subjected to a pretreatment period of 2 h. During this period, they were exposed to either a solution containing PFO with 0.03% Tween-80 at a concentration of 0.5 μg/mL, 1.5 μg/mL, and 3.0 μg/mL or 0.03% Tween-80 or beclomethasone, or egg water (30 larvae in each group, unless otherwise indicated). Subsequently, the larvae were anesthetized after being treated with 0.02% tricaine (Yuanye Bio-Technology Co. Ltd., China), and then placed in petri dishes covered with a layer of 2% agarose. The Leica M165C stereomicroscope and a 1-mm sapphire blade manufactured by World Precision Instruments (USA) were used for amputation (He *et al.*, 2020). Following this, after amputation,

the zebrafish larvae were transferred to either a fresh solution of PFO or egg water for 4 h. Microscopic real-time observations were conducted to monitor neutrophil migration in zebrafish larvae. Referring to a previous study setting beclomethasone as a positive control drug (He *et al.*, 2020), this glucocorticoid drug exhibits extensive anti-inflammatory properties and efficiently inhibits neutrophil migration to inflammation site in the zebrafish tail fin model.

RNA-seq assay and transcriptomics analysis

To fully reflect the anti-inflammatory effects of PFO on zebrafish larvae, we selected the larval zebrafish exposed to the highest concentration of PFO as well as control and model group for RNA-seq analysis. More details on sample preparation and RNA extraction etc. are provided in Appendix 2 (Du *et al.*, 2023). The raw data from RNA-seq were processed utilizing the statistical software R (version 4.0.4). The Trimmomatic program was used to remove low-quality reads. The expression levels of gene fragments were standardized by using the transcripts per million (TPM) algorithm. Genes with TPM > 1 were generally considered to be expressed, and gene banks were screened based on this standard. DESeq was used for differential analysis of gene expression, and the screening conditions were as follows: |log2Fold change |> 0.585 with $P < 0.05$. For these differentially expressed genes (DEGs), gene ontology (GO; http://geneontology.org/) and Kyoto Encyclopedia of Genes and Genomes (KEGG; https://www.genome.jp/kegg/) analysis were performed to study alterations in functioning and pathway.

Metabolomics analysis

Based on the transcriptome, three groups (control, model, and 3.0 μg/mL of PFO treatment) were subjected to metabolome analysis to further explore metabolites related to inflammation regulation. More details on sample preparation and metabolite identification etc. are provided in Appendix 3 (Du *et al.*, 2023). The raw data were converted to the mzXML format and imported into XCMS (https://xcmsonline.scripps.edu/) for further processing. Then all datasets were analyzed by using MetaboAnalyst 6.0 (https://www.metaboanalyst.ca/) and subjected to principal component analysis (PCA). Criteria for the statistical significance of metabolite changes among the groups were VIP > 1 and $P < 0.05$.

Gene expression analysis

For gene expression analysis by reverse transcription-polymerase chain reaction (RT-PCR), 30 zebrafish larvae from each group were treated using the same method as described above. Larval zebrafish were grinded and the total RNA was extracted with TRIZOL reagent (Thermo Fisher Scientific, USA). RNA concentration was measured by absorbance in CLARIOstar (BMG LABTECH, Germany). Then we used reverse transcription kit (Tiangen Biotech Co. Ltd., China) to synthesize complementary DNA (cDNA) from 2 μg of RNA and diluted (1:10). The synthesis of cDNA was performed with SYBR Green system (Tiangen Biotech Co. Ltd., China) and CFX96 Deep Well Dx (Bio-Rad Laboratories, USA) in RT-PCR. The $2^{-\Delta\Delta Ct}$ method was used for quantification of gene transcription and the transcription level of β-actin was used to normalize the relative expression of other genes in all samples (Hedrera *et al.*, 2013; Pereira *et al.*, 2023). All primer sequences used in this study were selected from the literature as presented in Table 1. Additional details, such as product length, annealing temperature, etc., are provided in the Appendix of this study (Table A1). For all experiments, three independent replicates were performed. RT-PCR was used to measure the levels of TNF-α, IL-6, and IL-1β in each group.

Statistical analysis

All experiments were conducted in triplicate. The results were expressed as mean values ± standard error of the mean (SEM). Statistical analysis was performed using GraphPad Prism 9 by one-way ANOVA with Tukey's post hoc test. For measurements, $P < 0.05$ was considered statistically significant. Omics analysis was conducted using the tools included in the MetaboAnalyst 6.0 software program, which can be accessed at http://www.metaboanalyst.ca.

Results

Identification of volatile compounds in PFO

GC-MS was performed to characterize volatile compounds in PFO, and at least 34 volatile compounds were identified. The peak numbers were recorded according to the retention time and percentage of each compound (Table 2). Perilla ketone (PK; 42.41%) was discovered in maximum proportion, followed by caryophyllene (9.51%), dehydroelsholtzia ketone (8.01%), elsholtzia ketone (EK, 6.46%), and cis-α-bergamotene (6.18%). Additionally, three compounds were present at >2% in PFO, which were cis-bisabolene (3.18%), pentamethylbenzene (3.11%), and 3-methyl-2-prenyl furan (2.97%). The discovered volatile compounds are the main source of various biological activities of PFO (Ahmed, 2019; Hou *et al.*, 2022).

Table 1. Sequence of primers for RT-PCR analysis.

Gene	Forward primer sequence (5′→3′)	Reverse primer sequence (5′→3′)
β-actin	GCCAACAGAGAGAAGATGACACAG	CAGGAAGGAAGGCTGGAAGAG
TNF-α	ACCAGGCCTTTTCTTCAGGT	TTTGCCTCCGTAGGATTCAG
IL-6	GATGACAGTGAAGCTCTTGGACAC	CCGATTCAGTCTGACCGGAGATTG
IL-1β	TGGACTTCGCAGCACAAAATG	GTTCACTTCACGCTCTTGGATG
Glula	TACTGACGGACACCCCTTTG	CAACCTGGAACTCCCACTGAG
Pyya	ATGGCAATGATGAAGCTGTGG	TCACCACATGTAGGTATCATC

pyya: peptide YYa.

Table 2. Volatile compounds identified in *Perilla frutescens* essential oil.

No.	Compound	RT (min)	Concentration (%)	Formula	MW (g/mol)
1.	D-Limonene	11.131	0.91	$C_{10}H_{16}$	136.23
2.	3-methyl-2-prenylfuran	13.215	2.97	$C_{10}H_{14}O$	150.22
3.	3,7-dimethyl-1,6-nonadien-3-ol	13.319	1.72	$C_{11}H_{20}O$	168.28
4.	4-Isopropylbenzaldehyde	16.202	1.47	$C_{10}H_{12}O$	148.20
5.	Elsholtzia ketone	16.369	6.46	$C_{10}H_{14}O_2$	166.22
6.	2,3-Dimethyl-5-(2,6,10-trimethylundecyl) furan	16.736	0.43	$C_{20}H_{36}O$	292.50
7.	Perilla ketone	18.200	42.41	$C_{10}H_{14}O_2$	166.22
8.	L-perillaldehyde	18.552	0.55	$C_{10}H_{14}O$	150.22
9.	Egomaketone	19.017	0.66	$C_{10}H_{12}O_2$	164.20
10.	Dehydroelsholtzia ketone	19.301	8.01	$C_{10}H_{12}O_2$	164.20
11.	(E)-methyl geranate	19.684	0.27	$C_{11}H_{18}O_2$	182.26
12.	δ-elemene	20.077	0.43	$C_{15}H_{24}$	204.35
13.	Copaene	21.083	0.41	$C_{15}H_{24}$	204.35
14.	β-Bourbonene	21.326	0.39	$C_{15}H_{24}$	204.35
15.	β-Elemene	21.502	0.42	$C_{15}H_{24}$	204.35
16.	Caryophyllene	22.359	9.51	$C_{15}H_{24}$	204.35
17.	α-Humulene	23.104	1.16	$C_{15}H_{24}$	204.35
18.	Cyclosativene	23.659	0.31	$C_{15}H_{24}$	204.35
19.	β-copaene	23.780	1.38	$C_{15}H_{24}$	204.35
20.	Cis-α-bergamotene	24.110	6.18	$C_{15}H_{24}$	204.35
21.	α-Muurolene	24.155	0.44	$C_{15}H_{24}$	204.35
22.	α-Farnesene	24.362	0.90	$C_{15}H_{24}$	204.35
23.	(+)-δ-cadinene	24.787	0.67	$C_{15}H_{24}$	204.35
24.	1,6,7-Trimethylnaphthalene	25.662	0.31	$C_{15}H_{24}$	170.25
25.	Spathulenol	26.104	0.36	$C_{15}H_{24}O$	220.35
26.	Caryophyllene oxide	26.257	1.00	$C_{15}H_{24}O$	220.35
27.	Cis-bisabolene	26.514	3.18	$C_{15}H_{24}$	204.35
28.	2,2',5,5'-Tetramethylbiphenyl	29.004	0.30	$C_{16}H_{18}$	210.31
29.	1,2,3,4-Tetrahydro-9-propylanthracene	30.448	0.30	$C_{17}H_{20}$	224.34
30.	4-methyl-2-prop-2-enyl-phenol	31.504	0.28	$C_{10}H_{12}O$	148.20
31.	Pentamethylbenzene	35.446	3.11	$C_{11}H_{16}$	148.25
32.	Androst-5-ene-3β,19-diol 3-acetate	35.758	0.31	$C_{21}H_{32}O_3$	332.48
33.	2-Allyl-4-methylphenol	36.295	1.30	$C_{10}H_{12}O$	148.20
34.	2-Furoic acid,2,6-dimethylnon-1-en-3-yn-5-yl ester	36.471	1.17	$C_{16}H_{20}O_3$	260.33
Total compounds					99.68

RT: retention time; MW: molecular weight.

PFO demonstrates anti-inflammatory effect in zebrafish tail fin amputation model

To evaluate the safety dose of PFO in zebrafish, we first tested Tween-80 at a volume ratio of 0.02–0.06% to obtain a concentration that was both safe and able to dissolve PFO. As shown in Figure 1A, for Tween-80 concentrations below 0.05%, the survival percentage of zebrafish larvae within 96 h exceeded 80%. Therefore, we selected 0.03% Tween-80 to dissolve PFO. Subsequently, we conducted tests for PFO at concentrations ranging from 0.3 to 3.0 μg/mL. The results, as depicted in Figure 1B, demonstrated that these doses were deemed safe for zebrafish larvae based on the observed survival rates.

In order to examine anti-inflammatory effect *in vivo*, we performed tests utilizing three distinct concentrations of PFO, as outlined previously. In addition, we employed glucocorticoid beclomethasone as a positive compound at a concentration of 25 μM (He *et al.*, 2020). Our findings indicated that PFO, at concentrations of 1.5 μg/mL and above, effectively suppressed neutrophil migration to the amputation site in zebrafish larvae, comparable to the inhibitory impact of beclomethasone. Furthermore, the inhibitory effect of PFO was directly proportional to the dosage administered, as shown in Figure 1C. The accumulation of neutrophils after trail fin amputation is shown in Figure 1D.

In order to further examine the anti-inflammatory impact of PFO in the tail fin amputation assay, we assessed messenger RNA (mRNA) levels of three immune-related genes using RT-PCR 4 h post-amputation in each experimental group. Three of the examined genes encoded

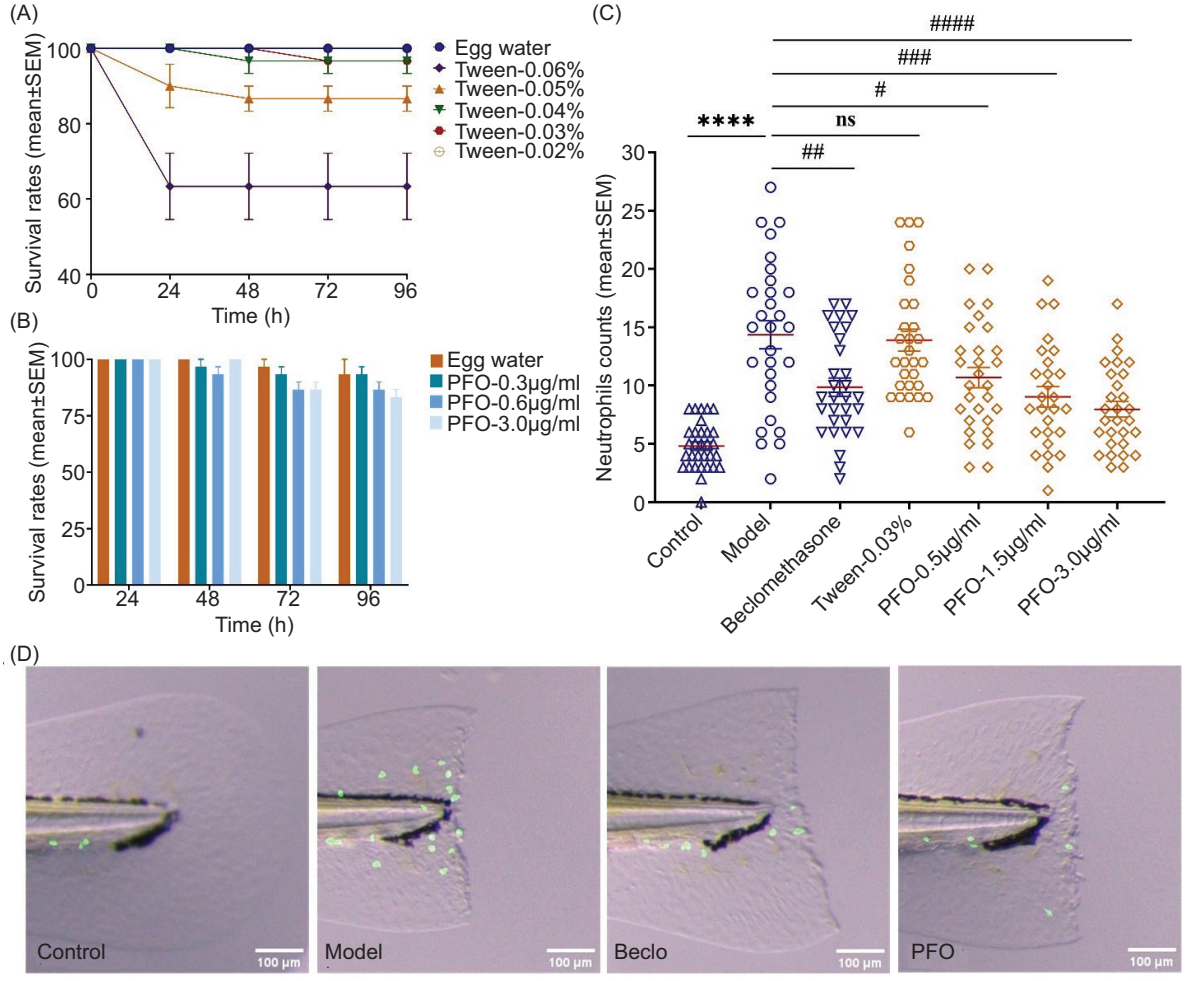

Figure 1. Effect of different treatments on neutrophil recruitment in the zebrafish tail fin amputation assay. Safety evaluation results of (A) Tween-80 and (B) PFO. (C) The number of neutrophils at amputation site 4 h after amputation upon treatment with beclomethasone (Beclo), Tween-80, and different concentrations of PFO. (D) The fluorescence microscopy images of wound-induced migration of neutrophils, which merge with white light images, in combination with control, model, beclomethasone (Beclo), and PFO treatments. *Model versus control, ****$P < 0.0001$; #treatment versus model, #$P < 0.05$, ##$P < 0.01$, ###$P < 0.001$, ####$P < 0.0001$; ns: no significant difference.

proinflammatory cytokines: TNF-α, IL-6, and IL-1β. The findings indicated that concentration of 3.0 μg/mL of PFO had the most effective regulatory impact on the production of proinflammatory cytokines, as shown in Figure 2. Consistent with the findings of bioactivity test, PFO had a regulatory influence on the production of proinflammatory cytokines that varied depending on the dose. Both PFO and beclomethasone exhibited the most pronounced modulation of TNF-α and IL-1β expression as compared to the model group. The presence of 0.5-μg/mL PFO did not have any impact on the regulation of IL-6 expression. Thus, we opted for a test dose of 3.0 μg/mL for further omics studies. These results indicate that PFO had a significant modulating effect on immune cells and pro-inflammatory cytokines, which provided strong evidence for the anti-inflammatory effects of PFO.

Transcriptomics analysis demonstrates that PFO regulates the patterns of gene expression in zebrafish

Through transcriptomics analysis, we identified more than 26,000 genes expressed differentially between the control, model, and PFO treatment groups. Next, unsupervised PCA was utilized to characterize differential profiling between these three groups. Figure 3A displays PCA results; there was a significant separation, and the contribution degree of PC1 and PC2 was 60.7% and 34.76%, respectively. Using a threshold of |log2FoldChange| > 0.585 and $P < 0.05$, we identified DEGs between these groups. As shown in Figures 3B and 3C, we performed a comparison of the differential gene expression between the model and control groups as well as between the PFO and model groups. The model

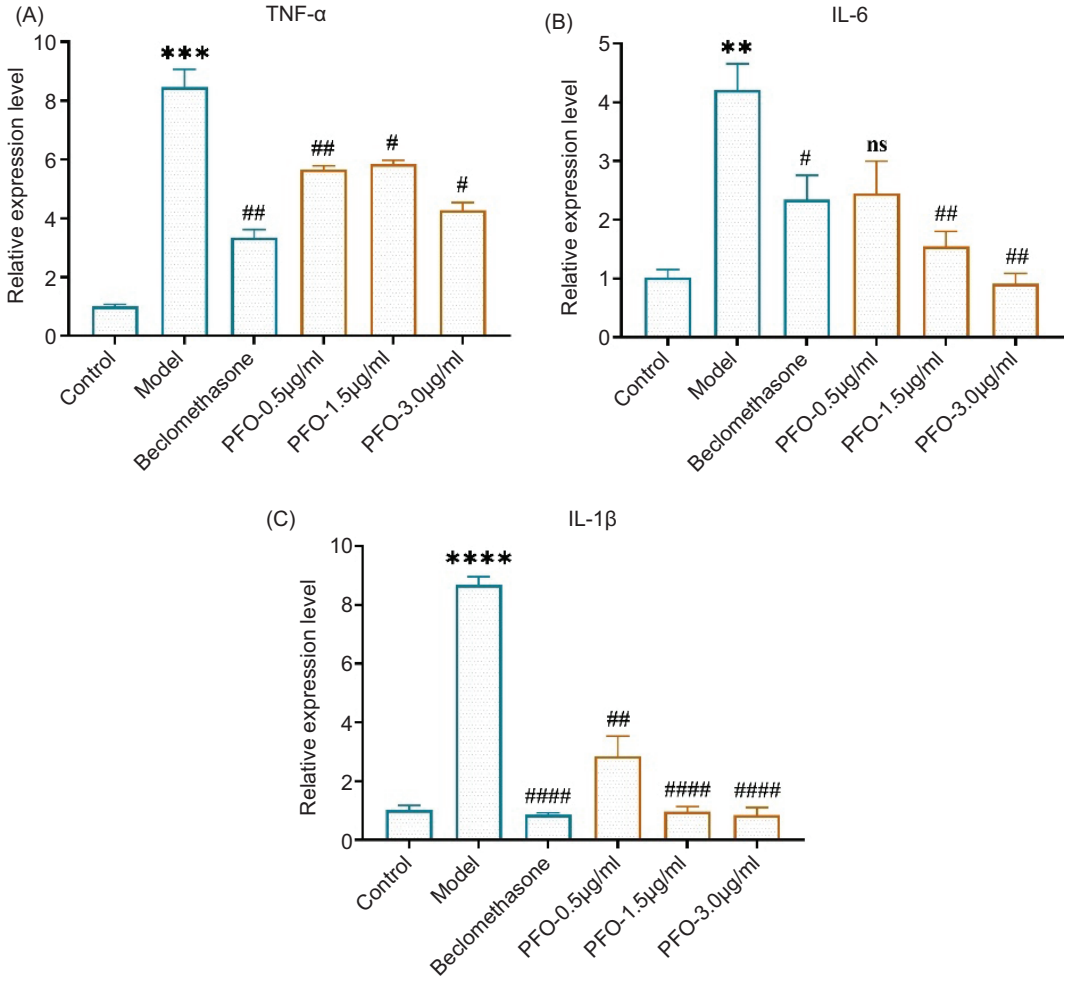

Figure 2. PFO regulates gene expression related to inflammation. Expression levels of pro-inflammatory cytokines—(A) TNF-α, (B) IL-6, and (C) IL-1β—were quantified with RT-PCR. Expression was normalized by comparison with the housekeeping gene β-*actin*. Bars represent mean values ± SEM of three independent experiments (each with technical duplicates). **$P < 0.01$, ***$P < 0.001$, ****$P < 0.0001$, compared with the control group. $^{\#}P < 0.05$, $^{\#\#}P < 0.01$, $^{\#\#\#\#}P < 0.0001$, compared with the model group; ns: no significant difference.

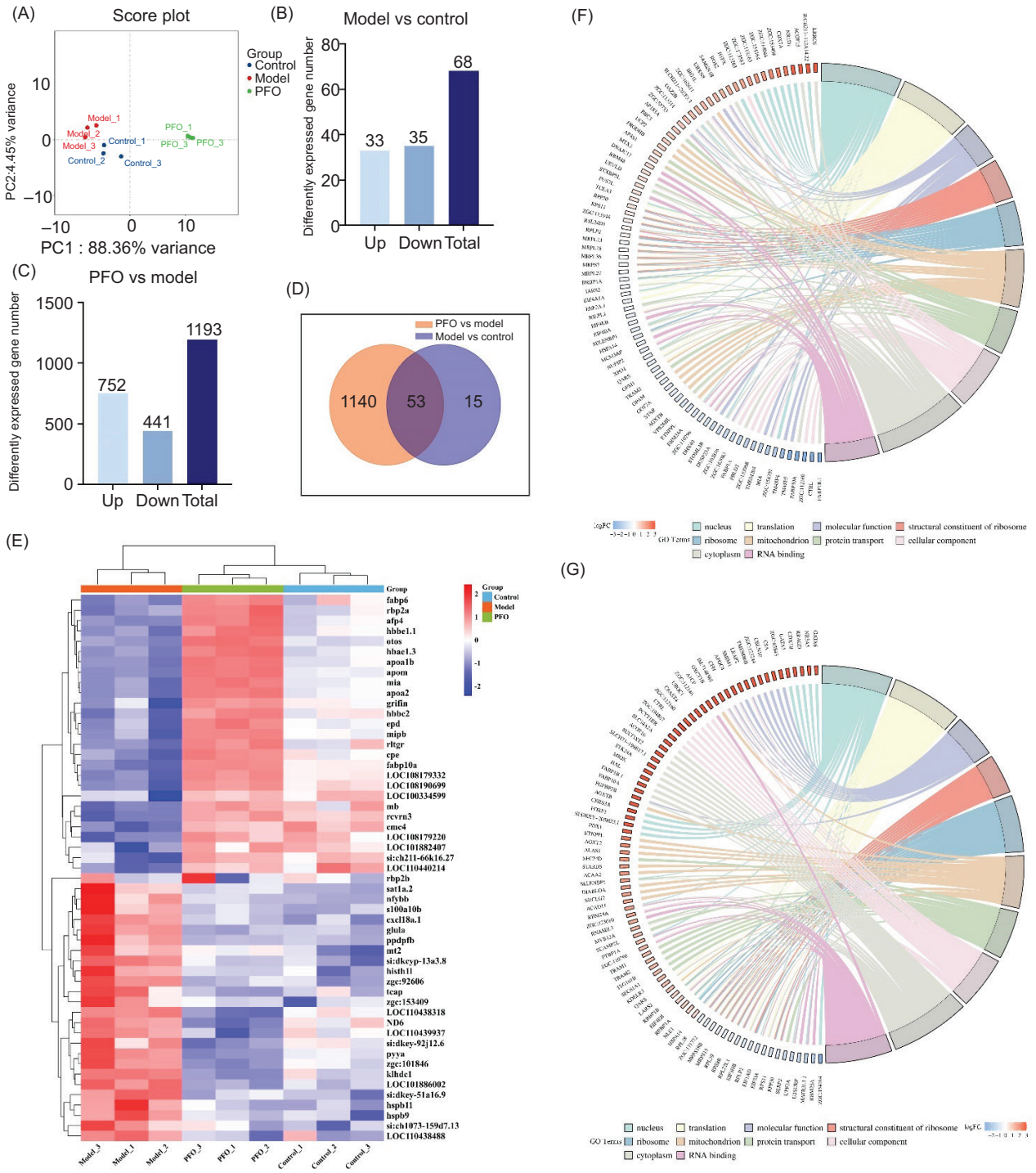

Figure 3. Transcriptome demonstrates that PFO modifies the patterns of gene expression in zebrafish. (A) PCA score plot. Blue, red, and green solid circles represent the control, model, and PFO groups, respectively. (B and C) Statistical analysis of the number of DEGs in model versus control and PFO versus model groups. (D) Veen diagram of model versus control group, and PFO versus model group. (E) Heat map of 53 DEGs altered in the control, model, and PFO treatment groups. (F) Chord diagram of model versus control group. (G) Chord diagram of PFO versus model group.

group showed differential expression of 68 genes, compared to the control group. Out of these genes, 33 exhibited increased (up-regulated) expression levels and 35 showed decreased (down-regulated) expression levels. Nevertheless, when comparing the PFO group and the model group, a grand total of 1,193 genes exhibited differential expression across the two groups. A total of 752 genes were found to be up-regulated whereas 441 genes were down-regulated. Subsequently, a Venn diagram was employed to graphically illustrate the outcomes of comparative analysis of DEGs across the two major cohorts: the model group compared to the control group, and the PFO group compared to the model group. Based on Figure 3D, 53 same DEGs were identified in two distinct cohorts, which were selected for subsequent studies.

A heatmap was used to visually depict regulatory patterns in 53 DEGs between the three groups, as shown in Figure 3E. To investigate the functional properties of these DEGs, a GO analysis was conducted. The study utilized a significance threshold of $P < 0.05$. The chord diagram provided a visual representation of the similarities and differences in gene function and regulatory patterns between two main groups: the model and control groups (Figure 3F) as well as the PFO and model groups (Figure 3G). Although the fundamental activities were identical in both groups, the model group showed significant alterations in the expression of a few genes, either down-regulated or down-regulated, compared to the control group. However, in comparison to the model group, a significant number of genes exhibited up-regulation following PFO treatment, indicating interference with inflammatory response. In addition, we focused on the significant regulatory effects of PFO on two DEGs: *hspb9* and *hspb11*. As key members of the heat shock protein family, both these DEGs had crucial roles in regulating the body's immune process (Bakthisaran *et al.*, 2015; Liu *et al.*, 2022), which was further illustrated by our results.

Metabolomics analysis demonstrates that PFO regulates the patterns of metabolites in zebrafish

In order to thoroughly investigate the impact of PFO on metabolic levels, we conducted a comprehensive study of metabolites in the control, model, and PFO groups using a non-targeted metabolomics approach. A score plot (Figure 4A) was used to depict PCA pattern. Three unique groups were observed, indicating that treatment for PFO resulted in considerable differences in the metabolomics profiles of zebrafish. PC1 accounted for 62.5% of variance, while PC2 accounted for 19% variance. Using the criterion of VIP > 1.0 and $P < 0.05$, we conducted screening and comparison of differentially expressed metabolites (DEMs) between groups. As shown in Figures 4B and 4C, we conducted a comparison of the number of DEMs between model and control groups as well as between PFO and model groups. In comparison to the control group, the model group exhibited regulation of 1,444 DEMs, with 75 up-regulated metabolites and 1,369 down-regulated metabolites. In the comparison between PFO and model groups, 1,217 DEMs were identified. Among these, 1,051 metabolites were up-regulated and 166 were down-regulated. Based on Figure 4D, 1,064 metabolites were screened, which were found to be common in two major cohorts. These metabolites were selected for further investigation. Next, a heatmap was generated to visually represent the findings of the comparative study of DEMs among three groups (Figure 4E). Evidently, the findings indicated that the administration of PFO treatment inclined to regulate parts of metabolites in a manner similar to the control group.

Combined multi-omics analysis reveals potential anti-inflammatory mechanism of PFO

In order to explore data from transcriptomics and metabolomics, we enriched the KEGG pathway through DEGs and DEMs screened by model versus control and PFO versus model in transcriptomics and metabolomics, respectively. The common KEGG pathway was identified by finding the intersection of analysis results from four pathways. A significant quantity of genes and metabolites in these pathways were acquired using reverse enrichment utilizing the same pathway function. These enriched genes and metabolites were compared with 53 DEGs and 1,064 DEMs, as shown in Table 3. When they are the same, they are the key DEGs and DEMs, and the pathway that could be compared with them could be defined as the key pathway.

Subsequently, we constructed a linked network comprising two key DEGs, 20 key DEMs, and four key pathways (Figure 5A). On the left, three key pathways were connected to more than half of the 20 key DEMs while connecting to one of the key DEGs. A big cluster of biomarkers responding to genes and metabolites was associated with amino acid and carbohydrate metabolism, which was primarily illustrated by key pathways, alanine, aspartate, and glutamate metabolism, arginine biosynthesis, and glyoxylate and dicarboxylate metabolism. On the right, only one key pathway, named neuroactive ligand–receptor interaction, which was critical and connected to the other half of the core DEMs and another of the key DEGs. Like a bridge, acetylaspartylglutamate (NAAG), glycine, succinate, pyruvate, and fumaric acid connect two key pathways at the same time, and it was evident that they played a crucial role in PFO regulating inflammatory response. Furthermore, aspartate and glutamine simultaneously intersected three crucial routes, which was readily apparent and important for deep exploration.

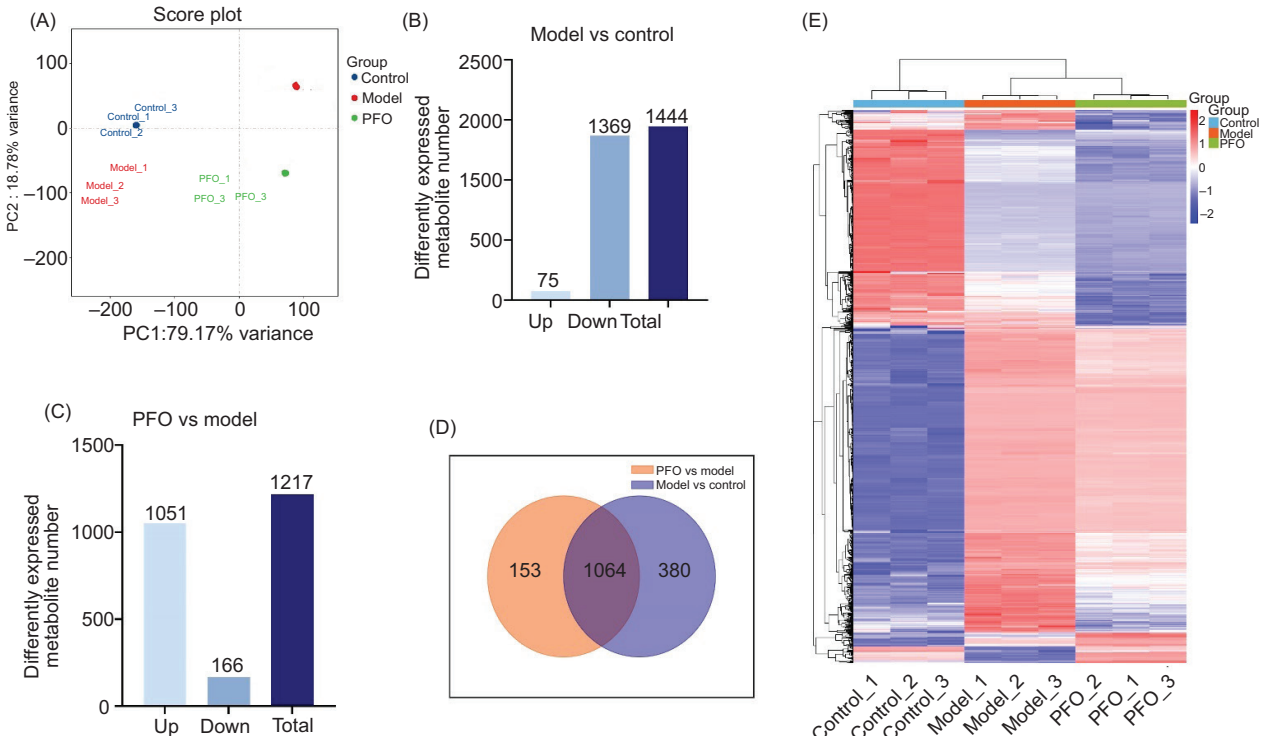

Figure 4. Metabolomics demonstrates that PFO modifies the patterns of metabolites in zebrafish. (A) PCA score plot. Blue, red, and green solid circles represent the control, model, and PFO groups, respectively. (B and C) Statistical analysis of the number of DEMs in model versus control and PFO versus model. (D) Veen diagram of DEMs between model versus control and PFO versus model. (E) Heatmap of 1,064 DEMs altered by control, model, and PFO treatment groups. DEMs: differentially expressed metabolites.

The alteration of these key DEMs at metabolic levels are shown in Figures 5B–5V. Heatmaps were performed to illustrate differences between three groups in the regulatory trends of key DEMs on metabolic level (Figure 5B). There were 16 DEGs that showed significant down-regulation, as illustrated in Figures 5C–5R. Some examples of these DEGs are pyruvate, adenosine, NAAG, and cis-aconitic acid. In addition, the up-regulation of taurine, acetylcholine, glycine, and aspartate was observed, as shown in Figures 5S–5V.

For two main DEGs, as shown in the network diagram (Figure 5A), *glula* was connected to three core pathways whose encoded proteins were directly related to the key DEM, glutamine, while the presence of *pyya* was significantly associated with neuroregulation. In addition, *pyya* was usually concerned with endocrine systems, and *glula* was predominantly expressed in astrocyte precursors and astrocytes in zebrafish brain. For further investigation into their role in the regulation of inflammation by PFO, we used RT-PCR to detect the expression levels of two genes in different groups, as shown in Figure 6. The expression level of *glula* and *pyya* were significantly affected by different concentrations of PFO. Both *glula* and *pyya* regulated inflammatory responses by reducing their expression levels. These results suggested that the regulatory impact of PFO on zebrafish inflammation model was directly associated with *glula* and *pyya* at the basal level.

Discussion

Effects on inflammatory markers

Perilla frutescens (L.) Britt, a traditional Chinese medicine, has a long history of treating various ailments. Chinese Pharmacopoeia records that it can be used to treat cold, cough, nausea, and vomiting as well as fish and crab poisoning. Based on the content of main volatile oil in *Perilla frutescens*, the plants are categorized into monoterpene (MT) and phenylpropylene (PP) types (Wu *et al.*, 2023). The MT-type plants are composed of seven subtypes, such as perillaldehyde (PA), PK, citral (C; a mixture of neral and geranial), perillen (PL), piperitenone (PT), shisofuran (SF), and elsholtzia ketone. Owing to the high percentage of PK (42.41%), the PFO utilized in the experiment was categorized as the PK sub-type. Therefore, our assessment and investigation of its anti-inflammatory properties were restricted to this specific sub-category. In

Table 3. Significantly changed genes, metabolites, and pathways revealed by transcriptomics and metabolomics analyses.

Pathway	Transcriptomics			Metabolomics			
	Model vs Control	PFO vs Model		Model vs Control		PFO vs Model	
Arginine biosynthesis	***glula*↑**	***glula*↓**		**Aspartate↓**	**Citrulline↓**	**Aspartate↑**	**Citrulline↑**
		glud1a↑	glud1b↑	**Fumaric acid↓**	**Glutamine↓**	**Fumaric acid↑**	**Glutamine↑**
		got2a↑	gpt2l↑	Glutamate↓	Alpha-KG↓		
		got1↑		N-Acetylglutamic acid↓			
				Argininosuccinic acid↓			
Alanine, aspartate and glutamate metabolism	***glula*↑**	***glula*↓**		**Asparagine↓**	**Aspartate↓**	**Asparagine↑**	**Aspartate↑**
		adssl1↑	agxta↑	**Adenylsuccinic acid↓**		**Adenylsuccinic acid↑**	
		agxtb↑	glud1b↑	**Fumaric-acid↓**	**Glutamine↓**	**Fumaric acid↑**	**Glutamine↑**
		glud1a↑	got1↑	**NAAG↓**	**Pyruvate↓**	**NAAG↑**	**Pyruvate↑**
		got2a↑	gpt2l↑	**Succinate↓**	Alpha-KG↓	**Succinate↑**	
				Argininosuccinic acid↓			
				Alanine↓	GABA↓		
				Glutamate↓			
Glyoxylate and dicarboxylate metabolism	***glula*↑**	***glula*↓**		**cis-Aconitic acid↑**		**cis-Aconitic acid↑**	
		acat1↑	aco2↑	**Glutamine↓**	**Glycine↓**	**Glutamine↑**	**Glycine↑**
		agxta↑	agxtb↑	**Mesaconic acid↓**		**Mesaconic acid↑**	
		cat↑	cs↑	**Pyruvate↓**	**Succinate↓**	**Pyruvate↑**	**Succinate↑**
		gcshb↑	grhprb↑	alpha-KG↓	Glutamate↓		
		hao1↑					
Neuroactive ligand–receptor interaction	***pyya*↑**	***pyya*↓**	adcyap1b↓	UTP↑		**Acetylcholine↑**	**ADP↑**
		calca↓	ccka↓	**Acetylcholine↓**	**ADP↓**	**Adenosine↑**	**Aspartate↑**
		crhb↓	glrbb↓	**Adenosine↓**	**Aspartate↓**	Dopamine↑	**Epinephrine↑**
		gnrh2↓	NPY↓	**Epinephrine↓**	**Glycine↓**	**Glycine↑**	**NAAG↑**
		pth1a↓	sst1.1↓	**NAAG↓**	**PGD2↓**	**PGD2↑**	**PGE2↑**
		sst3↓	tac1↓	**PGE2↓**	**Taurine↓**	PGI2↑	**Taurine↑**
		tac3a↓	tac3b↓	**UDP↓**	Glutamate↓	GABA↑	**UDP↑**
		vip↓	agt↑	beta-Alanine↓			
		c3a.1↑	f2↑	Leukotriene D4↓			
		gh1↑	insl5a↑				
		kng1↑	plg↑				
		prss59.2↑	try↑				
		tspo↑	vipb↑				

'↑': upregulating in model or PFO group, compared to the control or model group; '↓': downregulating in the model or PFO group, compared to the control or model group. Terms in bold are significantly changed in both comparison groups: model vs control and PFO vs model.
GABA: 4-aminobutyric acid; NAAG: N-acetylaspartylglutamate; NPY: neuropeptide Y; PGD2: prostaglandin D2; PGE2: prostaglandin E2; *pyya*: peptide YYa; UDP: uridine 5'-diphosphate; UTP: uridine 5'-triphosphate.

recent years, according to modern biological and pharmacological research on *Perilla frutescens*, this medicinal and edible plant exhibits a variety of biological activities, which are meticulously assessed using cell models. The anti-inflammatory activity of PK-type monoterpenoid via inhibiting inflammatory mediator and pro-inflammatory cytokines (TNF-α, IL-1β, and IL-6) in lipopolysaccharide-stimulated RAW264.7 cells (Zi *et al.*, 2021), the outcomes of this investigation supported our *in vivo* findings. In addition, PFO effectively controlled neuro-inflammatory responses by lowering the plasma levels of IL-1, IL-6, and TNF-α in a mice model (Hou *et al.*, 2022). Moreover, it demonstrated efficacy in reducing reflux oesophagitis in a mice model (Hou *et al.*, 2022). The results of these studies on inflammation in mammals also corroborated our findings.

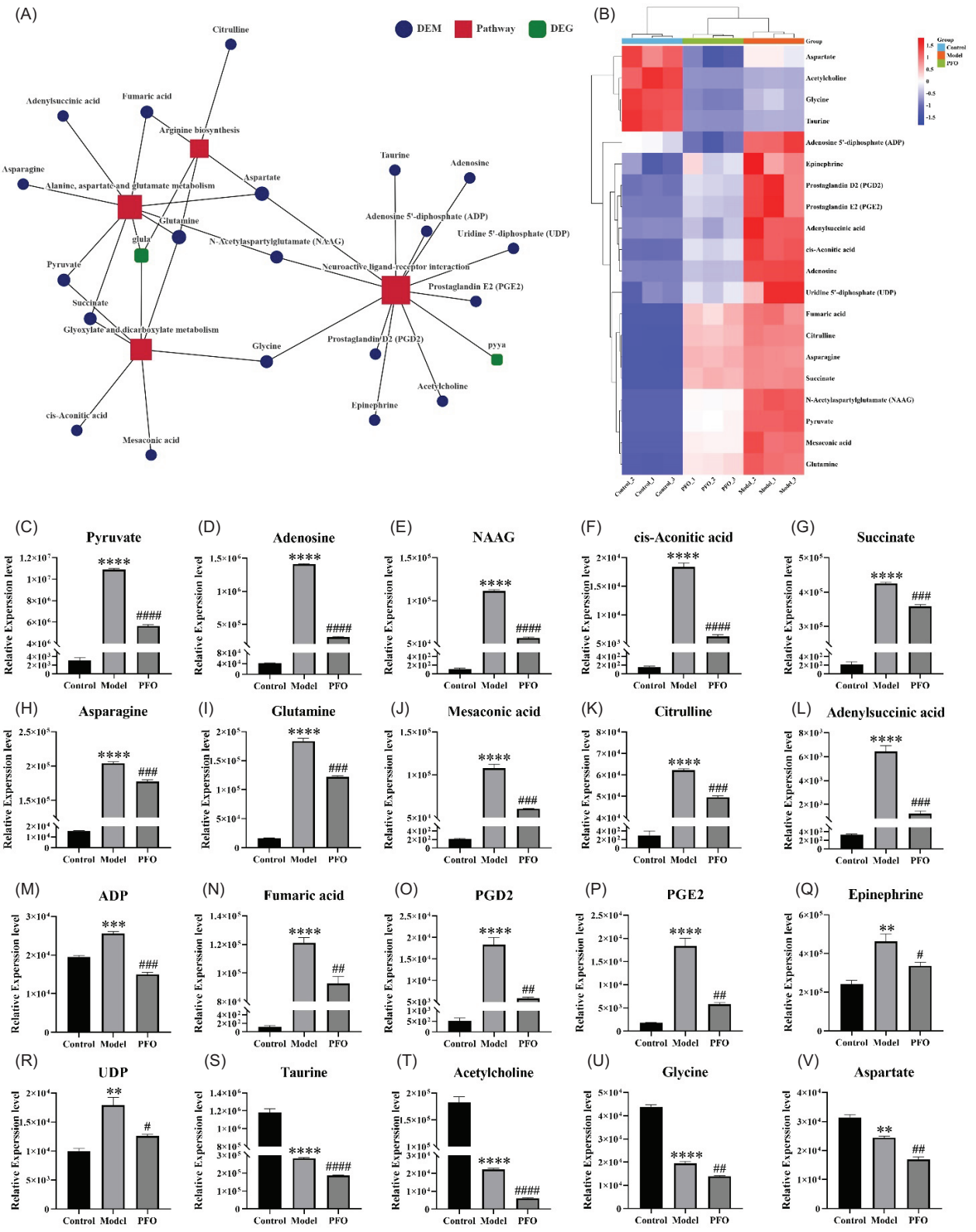

Figure 5. Analysis results of combined omics. (A) Interaction network of core pathway with key genes and metabolites. Blue solid circle, green solid rounded rectangle, and red rectangle represent DEMs, DEGs and core pathways, respectively. Line length and icon position have no actual purpose. (B) Heatmap of key metabolites altered by the control, model, and PFO treatment. (C–V) Alteration of these DEMs at metabolic level. Bars represent mean ± SEM of three independent experiments. **$P < 0.01$, ***$P < 0.001$, and ****$P < 0.0001$, compared with the control group. $^{\#}P < 0.05$, $^{\#\#}P < 0.01$, $^{\#\#\#}P < 0.001$, and $^{\#\#\#\#}P < 0.0001$, compared with the model group. DEGs: differentially expressed genes.

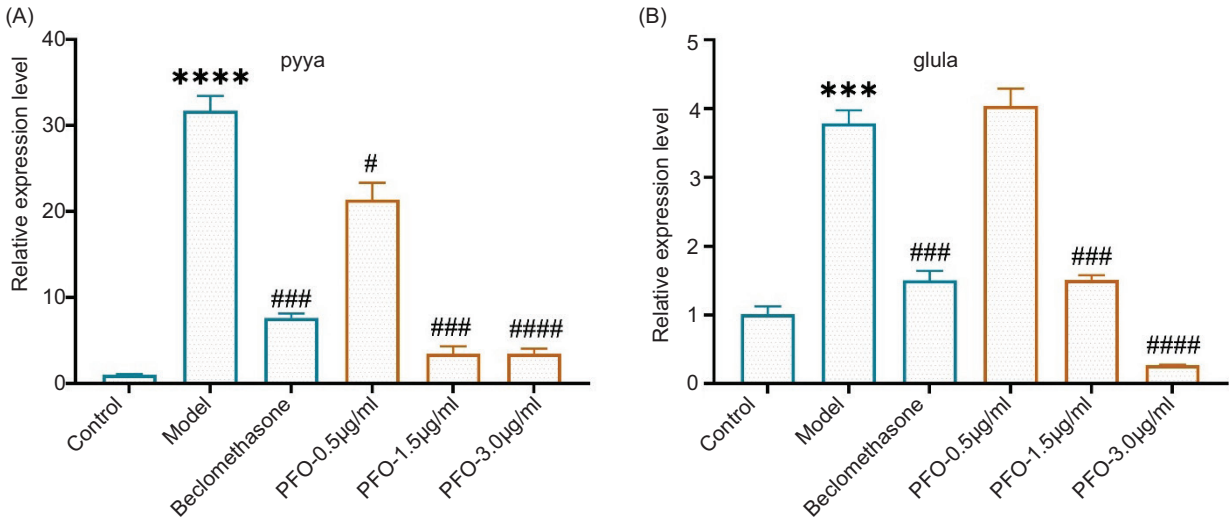

Figure 6. Relative messenger RNA (mRNA) expression levels of genes *pyya* and *glula* were verified by RT-PCR. (A) *pyya*, (B) *glula*. Bars represent mean ± SEM of three independent experiments (each with technical duplicates). ***$P < 0.001$, ****$P < 0.0001$, compared to the control group. $^{\#}P < 0.05$, $^{\#\#\#}P < 0.001$, $^{\#\#\#\#}P < 0.0001$, compared to the model group; ns: no significant difference.

Role of DEMs and DEGs

Moreover, the combined application of zebrafish model and multi-omics technology provided more possibilities for in-depth analysis of the mechanism of phytomedicine in many disease models (Liu *et al.*, 2024; Wang *et al.*, 2024). In this study, transcriptomics and metabonomics helped us to screen out two DEGs and 20 DEMs to understand the anti-inflammatory mechanism of PFO in zebrafish model. As a key DEG, peptide YYa (*pyya*) is a member of the neuropeptide Y family (NPY), which is expressed in the brain of zebrafish, particularly in the hypothalamus and pituitary (Larhammar and Bergqvist, 2013).

NPY and its receptors have a crucial role in controlling significant biological and pathological processes, including blood pressure, neuroendocrine secretion, seizures, neuronal excitability, and neuroplasticity (Chandrasekharan *et al.*, 2013). Furthermore, the protein encoded by *glula* belongs to the glutamine synthetase family. It catalyzes the synthesis of glutamine from glutamate and ammonia in an ATP-dependent reaction. Glutamine is a potent anti-inflammatory agent and can reduce both systemic and gut elaboration of proinflammatory cytokines (de Oliveira *et al.*, 2016). Our investigation revealed that both *pyya* and *glula* exhibited down-regulation following PFO administration, effectively suppressing inflammation. These data clearly indicate the likely mechanism of PFO's anti-inflammatory impact in zebrafish.

These key DEMs are reported to participate in the modulation of particular inflammation-related molecules or mediators (NAAG, pyruvate, glutamin, PGE2, etc), oxidative stress (succinate and PGD2), growth and development of zebrafish (especially in relation to angiogenesis, glycine, and PGE2) and had a crucial role in neuroactive protective effect (asparagine, acetylcholine, epinephrine, fumatic acid, etc) (Zheng, 2009). Prior studies noted the importance and different functions of these DEMs related to inflammatory responses in the zebrafish tail fin model. For example, PGE2 facilitated the clearance of neutrophils by promoting reverse migration. Moreover, elevation of the lactate pathway following tissue amputation involved the conversion of pyruvate to lactate, while a deficiency in calcium-dependent citrullination resulted in impaired resolution of inflammation and regeneration (Golenberg *et al.*, 2020; Scott *et al.*, 2022).

Additionally, a study conducted on mice models investigated the effects of administering inhibitors of enzymes that deactivated NAAG on the reduction of responses to inflammatory pain (Adedoyin *et al.*, 2010). In another study, glutamine was found to ameliorate lipopolysaccharide-induced acute lung injury in mice by mediating the toll-like receptor–mitogen-activated protein kinase (TLR4/MAPK) signaling pathway (Huang *et al.*, 2021).

The aforementioned metabolites had a pivotal role in inflammatory response and exhibited a considerable down-regulation in metabolomics results. Furthermore, half of the 20 DEMs are either neurotransmitters or have a direct connection to them. In this study, epinephrine, glutamine, adenosine, adenosine 5'-diphosphate (ADP), and fumaric acid affected inflammation by regulating trends of the control group, and acetylcholine, asparagine, glycine, and taurine affect inflammation by significantly decreased expression level, compared to the

model group. This finding broadly supports the work of other studies in this area, linking neurotransmitters with inflammation (Nguyen *et al.*, 2024a; Soares *et al.*, 2022; Wu *et al.*, 2019). PFO reverted the regulation tendency of these metabolites by significantly creating huge opportunities for further research.

Metabolic pathways

In this research, arginine biosynthesis, alanine, aspartate, and glutamate metabolism, glyoxylate and dicarboxylate metabolism, and neuroactive ligand–receptor interaction are the most important pathways enriched by core DEGs and DEMs. Multiple studies have demonstrated the significant involvement of arginine biosynthesis and alanine, aspartate, and glutamate metabolism in the body's inflammatory and immunological responses (Miyajima, 2020; Zaccherini *et al.*, 2021; Zhang *et al.*, 2022). For instance, it was discovered that arginine was identified as a pivotal regulator of body's immune response; its availability, synthesis, and catabolism are intricately interconnected elements of immune responses, and their fine-tuning can determine varying pro-inflammatory or anti-inflammatory outcomes (Martí i Líndez and Reith, 2021). Our results confirmed that PFO interferes with inflammation by regulating amino acid metabolism, carbohydrate metabolism as well as neuroactive ligand–receptor interaction. Nguyen *et al.* employed network pharmacology methods to forecast the KEGG pathways associated with the therapeutic effects of PFO on nervous system disorders (Nguyen *et al.*, 2024a). The authors also identified neuroactive ligand–receptor interaction as a potentially significant target of essential oil. This discovery reinforced our findings and strongly suggested that PFO regulated inflammation by modulating the neuroactive ligand–receptor interaction pathway. This indicated that future research could concentrate on investigating the correlation between nervous system regulation and inflammation in the tail fin of zebrafish. These investigations could delve further into the neural and inflammatory mechanisms that interact during the healing of tail fin tissue.

Broader perspectives

Our experiment was straightforward and visually revealed the anti-inflammatory activity of PFO, which relied on the zebrafish embryos having the ability to efficiently absorb small molecules quickly. The combination of complicated gene editing and live high-resolution imaging in zebrafish models allowed for the study and documentation of developmental progress and illnesses with unparalleled molecular precision and resolution (Huang *et al.*, 2018). The development and widespread use of zebrafish models provide improved prospects for evaluating the biological efficacy of natural products and their key active components (Lin *et al.*, 2022). In addition, by using the zebrafish model, the safety and bioactivity of many essential oils are evaluated extensively, such as developmental toxicity (da Silva *et al.*, 2023), anxiolytic properties (Batista *et al.*, 2024; Silveira *et al.*, 2022), and impact on angiogenesis (Elsayed *et al.*, 2020). For studying the essential oil's anti-inflammatory effects, the researchers found that *Artemisia vulgaris* essential oil could enhance the gut's immunological function by controlling oxidative stress by using a zebrafish IBD model (Meng *et al.*, 2022). Moreover, several studies employed an adult zebrafish model of induced inflammation to evaluate the anti-inflammatory properties of essential oils (Pereira *et al.*, 2024). In our study, by using the tail fin amputation model in larval zebrafish, we discovered that the anti-inflammatory effects of PFO were directly linked to the regulation of neutrophils. The zebrafish model is characterized by its rapid and efficient nature, making it a valuable tool for evaluating the anti-inflammatory activity of PFO and complements other animal models. In the future, for different categories and subtypes of *Perilla*, zebrafish models could be used to study the difference in biological activity caused by differences in its main essential oil components to explore further the potential application value of PFO in anti-inflammatory drug.

Conclusions

In this research, we revealed that PFO exhibits robust anti-inflammatory properties by effectively suppressing aggregation of neutrophils and lowering the expression of pro-inflammatory genes. Furthermore, we observed a correlation between the anti-inflammatory effect of PFO and the regulation of neural activity by using the combination of transcriptomics and metabolomics. These findings indicate that PFO regulates inflammation by modulating the neuroactive ligand–receptor interaction pathway, advancing our understanding of essential oil-mediated molecular mechanisms of inflammation, paving the way for novel natural therapeutics. However, the limited relevance of zebrafish model to human inflammatory responses necessitates validation in more intricate systems. Assessing the anti-inflammatory properties of PFO would enhance our comprehension and advancement of the medicinal and practical benefits of *Perilla frutescens*. Future research on PFO should continue with multi-omics studies to explore additional metabolic pathways and validation in mammalian models to assess clinical potential.

Data Availability Statement

The datasets used in this study are available from the corresponding author upon reasonable request.

Acknowledgments

The authors thank Zhongfeng Chen and Guanshu Biotechnology Services (Changchun) Co., Ltd. provided the technical guidance.

Author Contributions

Yao Fu: writing—original draft, methodology, investigation, data curation, formal analysis, visualization, and validation; Jie Cheng: methodology, investigation, data curation, formal analysis, visualization, and validation. Xianghe Meng: resources; Guicai Tang: resources and fund acquisition; Li Li: investigation; Ziyoviddin Yusupov: writing—review and editing; Komiljon Tojibaev: writing—review and editing; Min He: conceptualization, writing—review and editing, supervision, and funding acquisition; Mengmeng Sun: conceptualization, writing—review and editing, supervision, funding acquisition. All authors had read and agreed to the published version of the manuscript.

Conflict of Interest

The authors declared that they had no known competing financial interests or personal relationships that could have appeared to influence the work reported in this paper.

Funding

This research was financially supported by the Scientific and Technological Developing Project of Jilin Province (No. YDZJ202301ZYTS151); the Open Scientific Project of Institute of Basic Theory for Chinese Medicine, China Academy of Chinese Medical Sciences (No. YZX-202207); the Pilotscale Selection Project of Colleges and Universities in Changchun City (No. 24GXYSZZ10); and the Ministry of Human Resources and Social Security of the People's Republic of China High-Level Talent Project (Nos. 030102070 and 030102071).

References

Adedoyin, M.O., Vicini, S., and Neale, J.H., 2010. Endogenous N-acetylaspartylglutamate (NAAG) inhibits synaptic plasticity/transmission in the amygdala in a mouse inflammatory pain model. Molecular Pain 6: 18. http://doi.org/10.1186/1744-8069-6-60

Ahmed, H.M., 2019. Ethnomedicinal, Phytochemical and Pharmacological Investigations of *Perilla frutescens* (L.) Britt. Molecules 24(1): 102. http://doi.org/10.3390/molecules24010102

Ahmed, H.M., and Al-Zubaidy, A.M.A., 2020. Exploring natural essential oil components and antibacterial activity of solvent extracts from twelve *Perilla frutescens* L. genotypes. Arabian Journal of Chemistry 13(10): 7390–7402. http://doi.org/10.1016/j.arabjc.2020.08.016

Bakthisaran, R., Tangirala, R., and Rao, C.M., 2015. Small heat shock proteins: Role in cellular functions and pathology. Biochimica et Biophysica Acta (BBA) - Proteins and Proteomics 1854(4): 291–319. https://doi.org/10.1016/j.bbapap.2014.12.019

Batista, F.L.A., de Araújo, S.M.B., de Sousa, D.B., Sobrinho, F.B.C., de Lima Silva, M.G., de Oliveira, M.R.C., da Costa, R.H.S., Rodrigues, L.B., Bezerra, F.S., de Azevedo, D.V., Vieira-Neto, A.E., Magalhães, F.E.A., and de Menezes, I.R.A., 2024. Anticonvulsant and anxiolytic-like potential of the essential oil from the Ocimum basilicum Linn leaves and its major constituent estragole on adult zebrafish (Danio rerio). Neurochemistry International 178: 105796. http://doi.org/10.1016/j.neuint.2024.105796

Campos-Sánchez, J.C., and Esteban, M.Á., 2021. Review of inflammation in fish and value of the zebrafish model. Journal of Fish Diseases 44(2): 123–139. http://doi.org/10.1111/jfd.13310

Chandrasekharan, B., Nezami, B.G., and Srinivasan, S., 2013. Emerging neuropeptide targets in inflammation: NPY and VIP. American Journal of Physiology-Gastrointestinal and Liver Physiology 304(11): G949–G957. http://doi.org/10.1152/ajpgi.00493.2012

Chen, C.Y., Leu, Y.L., Fang, Y., Lin, C.F., Kuo, L.M., Sung, W.C., Tsai, Y.F., Chung, P.J., Lee, M.C., Kuo, Y.T., Yang, H.W., and Hwang, T.L., 2015. Anti-inflammatory effects of *Perilla frutescens* in activated human neutrophils through two independent pathways: Src family kinases and Calcium. Scientific Reports 5: 11. http://doi.org/10.1038/srep18204

Choe, C.P., Choi, S.-Y., Kee, Y., Kim, M.J., Kim, S.-H., Lee, Y., Park, H.-C., and Ro, H., 2021. Transgenic fluorescent zebrafish lines that have revolutionized biomedical research. Laboratory Animal Research 37(1): 26. http://doi.org/10.1186/s42826-021-00103-2

Chopra, D., Shukla, S., Rana, P., Kamar, M.D., Gaur, P., Bala, M., and Pathaniya, D. 2024. Overview of Inflammation. In: Tripathi, A., Dwivedi, A., Gupta, S., and Poojan, S. (eds.) Inflammation Resolution and Chronic Diseases. Springer Nature, Singapore, pp. 1–18. https://doi.org/10.1007/978-981-97-0157-5_1

da Silva, I.I., da Silva, N.P.C., Marrs, J.A., and Cadena, P.G., 2023. Essential Oils Produce Developmental Toxicity in Zebrafish Embryos and Cause Behavior Changes in Zebrafish Larvae. Biomedicines 11(10): 2821. http://doi.org/10.3390/biomedicines11102821

de Oliveira, D.C., da Silva Lima, F., Sartori, T., Santos, A.C.A., Rogero, M.M., and Fock, R.A., 2016. Glutamine metabolism and its effects on immune response: molecular mechanism and gene expression. Nutrire 41(1): 14. http://doi.org/10.1186/s41110-016-0016-8

Ding, X., Yan, F., Wang, W., Qin, J., and Luo, L., 2024. Integration of transcriptomics and metabolomics identify biomarkers of aberrant lipid metabolism in ulcerative colitis. International Immunopharmacology 131: 111865. http://doi.org/10.1016/j.intimp.2024.111865

Du, B., Zhang, F., Zhou, Q., Cheng, W., Yu, Z., Li, L., Yang, J., Zhang, X., Zhou, C., and Zhang, W., 2023. Joint analysis of the metabolomics and transcriptomics uncovers the dysregulated network and develops the diagnostic model of high-risk neuroblastoma. Scientific Reports 13(1): 16991. http://doi.org/10.1038/s41598-023-43988-w

Elsayed, E.A., Farooq, M., Sharaf-Eldin, M.A., El-Enshasy, H.A., and Wadaan, M., 2020. Evaluation of developmental toxicity and anti-angiogenic potential of essential oils from Moringa oleifera and Moringa peregrina seeds in zebrafish (Danio rerio) model. South African Journal of Botany 129: 229–237. http://doi.org/10.1016/j.sajb.2019.07.022

Ghimire, B.K., Yoo, J.H., Yu, C.Y., and Chung, I.M., 2017. GC-MS analysis of volatile compounds of *Perilla frutescens* Britton var. *Japonica* accessions: morphological and seasonal variability. Asian Pacific Journal of Tropical Medicine 10(7): 705–714. http://doi.org/10.1016/j.apjtm.2017.07.004

Golenberg, N., Squirrel, J.M., Bennin, D.A., Rindy, J., Pistono, P.E., Eliceiri, K.W., Shelef, M.A., Kane, J., and Huttenlocher, A., 2020. Citrullination regulates wound responses and tissue regeneration in zebrafish. Journal of Cell Biology 219(4): 17. http://doi.org/10.1083/jcb.201908164

Gong, G., Chen, H., Kam, H., Chan, G., Tang, Y.-x., Wu, M., Tan, H., Tse, Y.-c., Xu, H.-x., and Lee, S.M.-y., 2020. In Vivo Screening of Xanthones from Garcinia oligantha Identified Oliganthin H as a Novel Natural Inhibitor of Convulsions. Journal of Natural Products 83(12): 3706–3716. http://doi.org/10.1021/acs.jnatprod.0c00963

He, M., Halima, M., Xie, Y.F., Schaaf, M.J.M., Meijer, A.H., and Wang, M., 2020. Ginsenoside Rg1 Acts as a Selective Glucocorticoid Receptor Agonist with Anti-Inflammatory Action without Affecting Tissue Regeneration in Zebrafish Larvae. Cells 9(5): 15. http://doi.org/10.3390/cells9051107

Hedrera, M.I., Galdames, J.A., Jimenez-Reyes, M.F., Reyes, A.E., Avendaño-Herrera, R., Romero, J., and Feijóo, C.G., 2013. Soybean Meal Induces Intestinal Inflammation in Zebrafish Larvae. PLOS ONE 8(7): e69983. http://doi.org/10.1371/journal.pone.0069983

Hou, T., Netala, V.R., Zhang, H., Xing, Y., Li, H., and Zhang, Z., 2022. *Perilla frutescens*: A Rich Source of Pharmacological Active Compounds. Molecules 27(11): 3578. http://doi.org/10.3390/molecules27113578

Huang, B.K., Lei, Y.L., Tang, Y.H., Zhang, J.C., Qin, L.P., and Liu, J.A., 2011. Comparison of HS-SPME with hydrodistillation and SFE for the analysis of the volatile compounds of Zisu and Baisu, two varietal species of *Perilla frutescens* of Chinese origin. Food Chemistry 125(1): 268–275. http://doi.org/10.1016/j.foodchem.2010.08.043

Huang, J., Liu, J., Chang, G., Wang, Y., Ma, N., Roy, A.C., and Shen, X., 2021. Glutamine supplementation attenuates the inflammation caused by LPS-induced acute lung injury in mice by regulating the TLR4/MAPK signaling pathway. Inflammation 44(6): 2180–2192. http://doi.org/10.1007/s10753-021-01491-2

Huang, J.J., Wang, Y.F., and Zhao, J.G., 2018. CRISPR editing in biological and biomedical investigation. Journal of Cellular Physiology 233(5): 3875–3891. http://doi.org/10.1002/jcp.26141

Ji, W.W., Li, R.P., Li, M., Wang, S.Y., Zhang, X., Niu, X.X., Li, W., Yan, L., Wang, Y., Fu, Q., and Ma, S.P., 2014. Antidepressant-like effect of essential oil of *Perilla frutescens* in a chronic, unpredictable, mild stress-induced depression model mice. Chinese Journal of Natural Medicines 12(10): 753–759. http://doi.org/10.1016/s1875-5364(14)60115-1

Larhammar, D., and Bergqvist, C.A., 2013. Ancient grandeur of the vertebrate neuropeptideY system shown by the coelacanth *Latimeria chalumnae*. Frontiers in Neuroscience 7: 10. http://doi.org/10.3389/fnins.2013.00027

Li, N., Zhang, Z.J., Li, X.J., Li, H.Z., Cui, L.X., and He, D.L., 2018. Microcapsules biologically prepared using *Perilla frutescens* (L.) Britt. essential oil and their use for extension of fruit shelf life. Journal of the Science of Food and Agriculture 98(3): 1033–1041. http://doi.org/10.1002/jsfa.8552

Lin, F.-J., Li, H., Wu, D.-T., Zhuang, Q.-G., Li, H.-B., Geng, F., and Gan, R.-Y., 2022. Recent development in zebrafish model for bioactivity and safety evaluation of natural products. Critical Reviews in Food Science and Nutrition 62(31): 8646–8674. http://doi.org/10.1080/10408398.2021.1931023

Lin, L.-Y., Peng, C.-C., Wang, H.-E., Liu, Y.-W., Shen, K.-H., Chen, K.-C., and Peng, R.Y., 2016. Active Volatile Constituents in Perilla frutescens Essential Oils and Improvement of Antimicrobial and Anti-Inflammatory Bioactivity by Fractionation. Journal of Essential Oil Bearing Plants 19(8): 1957–1983. http://doi.org/10.1080/0972060X.2016.1226962

Liu, J., Wan, Y., Zhao, Z., and Chen, H., 2013. Determination of the content of rosmarinic acid by HPLC and analytical comparison of volatile constituents by GC-MS in different parts of Perilla frutescens (L.) Britt. Chemistry Central Journal 7(1): 61. http://doi.org/10.1186/1752-153x-7-61

Liu, H., Yang, M., and Dong, Z., 2022. HSPB11 is a Prognostic Biomarker Associated with Immune Infiltrates in Hepatocellular Carcinoma. International Journal of General Medicine 15(null): 4017–4027. http://doi.org/10.2147/IJGM.S363679

Liu, F., Yang, Y., Dong, H., Zhu, Y., Feng, W., and Wu, H., 2024. Essential oil from Cinnamomum cassia Presl bark regulates macrophage polarization and ameliorates lipopolysaccharide-induced acute lung injury through TLR4/MyD88/NF-κB pathway. Phytomedicine 129: 155651. http://doi.org/10.1016/j.phymed.2024.155651

Makino, T., Furata, Y., Wakushima, H., Fujii, H., Saito, K., and Kano, Y., 2003. Anti-allergic effect of *Perilla frutescens* and its active constituents. Phytotherapy Research 17(3): 240–243. http://doi.org/10.1002/ptr.1115

Margraf, A., Ley, K., and Zarbock, A., 2019. Neutrophil Recruitment: From Model Systems to Tissue-Specific Patterns. Trends in Immunology 40(7): 613–634. http://doi.org/10.1016/j.it.2019.04.010

Martí i Líndez, A.-A., and Reith, W., 2021. Arginine-dependent immune responses. Cellular and Molecular Life Sciences 78(13): 5303–5324. http://doi.org/10.1007/s00018-021-03828-4

Masuda, A., Hidaka, K., Honda, S., Taniguchi, A., Doi, S., and Masuda, T., 2018. Radical Scavenging Properties of Roasted Egoma (Perilla frutescens var. frutescens) Oils and Identification of Their Characteristic Scavengers. Journal of Nutritional

Science and Vitaminology (Tokyo) 64(6): 466–472. http://doi.org/10.3177/jnsv.64.466

Meng, R., Wu, S., Chen, J., Cao, J., Li, L., Feng, C., Liu, J., Luo, Y., and Huang, Z., 2022. Alleviating effects of essential oil from Artemisia vulgaris on enteritis in zebrafish via modulating oxidative stress and inflammatory response. Fish & Shellfish Immunology 131: 323–341. http://doi.org/10.1016/j.fsi.2022.10.010

Miyajima, M., 2020. Amino acids: key sources for immunometabolites and immunotransmitters. International Immunology 32(7): 435–446. http://doi.org/10.1093/intimm/dxaa019

Ng, S.C., Shi, H.Y., Hamidi, N., Underwood, F.E., Tang, W., Benchimol, E.I., Panaccione, R., Ghosh, S., Wu, J.C.Y., Chan, F.K.L., Sung, J.J.Y., and Kaplan, G.G., 2017. Worldwide incidence and prevalence of inflammatory bowel disease in the 21st century: a systematic review of population-based studies. Lancet 390(10114): 2769–2778. http://doi.org/10.1016/s0140-6736(17)32448-0

Nguyen, L.T.H., Nguyen, N.P.K., Tran, K.N., Choi, H.J., Moon, I.S., Shin, H.M., and Yang, I.J., 2024a. Essential oil of *Pterocarpus santalinus L.* alleviates behavioral impairments in social defeat stress-exposed mice by regulating neurotransmission and neuroinflammation. Biomedicine & Pharmacotherapy 171: 11. http://doi.org/10.1016/j.biopha.2024.116164

Nguyen, L.T.H., Nguyen, N.P.K., Tran, K.N., Shin, H.M., and Yang, I.J., 2024b. Intranasal administration of the essential oil from Perillae Folium ameliorates social defeat stress-induced behavioral impairments in mice. Journal of Ethnopharmacology 324: 17. http://doi.org/10.1016/j.jep.2024.117775

Omari-Siaw, E., Wang, Q.L., Sun, C.Y., Gu, Z.Q., Zhu, Y., Cao, X., Firempong, C.K., Agyare, R., Xu, X.M., and Yu, J.N., 2016. Tissue distribution and enhanced *in vivo* anti-hyperlipidemic-antioxidant effects of perillaldehyde-loaded liposomal nanoformulation against Poloxamer 407-induced hyperlipidemia. International Journal of Pharmaceutics 513(1–2): 68–77. http://doi.org/10.1016/j.ijpharm.2016.08.042

Pavela, R., and Benelli, G., 2016. Essential Oils as Ecofriendly Biopesticides? Challenges and Constraints. Trends Plant Sci 21(12): 1000–1007. http://doi.org/10.1016/j.tplants.2016.10.005

Pereira, W.F., Everson da Silva, L., do Amaral, W., Andrade Rebelo, R., Quefi, B., Wlisses da Silva, A., et al. 2024. Essential Oils from the Genus Piper Promote Antinociception by Modulating TRP Channels and Anti-Inflammatory Effects in Adult Zebrafish. Chem Biodivers 21(3): e202301807. http://doi.org/10.1002/cbdv.202301807

Pereira, R.B., Rahali, F.Z., Nehme, R., Falleh, H., Jemaa, M.B., Sellami, I.H., Ksouri, R., Bouhallab, S., Ceciliani, F., Abdennebi-Najar, L., and Pereira, D.M., 2023. Anti-inflammatory activity of essential oils from Tunisian aromatic and medicinal plants and their major constituents in THP-1 macrophages. Food Research International 167: 112678. http://doi.org/10.1016/j.foodres.2023.112678

Reddy, N.V., Li, H.Z., Hou, T.Y., Bethu, M.S., Ren, Z.Q., and Zhang, Z.J., 2021. Phytosynthesis of Silver Nanoparticles Using *Perilla frutescens* Leaf Extract: Characterization and Evaluation of Antibacterial, Antioxidant, and Anticancer Activities. International Journal of Nanomedicine 16: 15–29. http://doi.org/10.2147/ijn.S265003

Scott, C.A., Carney, T.J., and Amaya, E., 2022. Aerobic glycolysis is important for zebrafish larval wound closure and tail regeneration. Wound Repair and Regeneration 30(6): 665–680. http://doi.org/10.1111/wrr.13050

Silveira, V., Santos Rubio, K.T., and Poleti Martucci, M.E., 2022. Anxiolytic effect of Anthemis nobilis L. (roman chamomile) and Citrus reticulata Blanco (tangerine) essential oils using the light-dark test in zebrafish (Danio rerio). Journal of Ethnopharmacology 298: 115580. http://doi.org/10.1016/j.jep.2022.115580

Soares, G., Bhattacharya, T., Chakrabarti, T., Tagde, P., and Cavalu, S., 2022. Exploring Pharmacological Mechanisms of Essential Oils on the Central Nervous System. Plants-Basel 11(1): 25. http://doi.org/10.3390/plants11010021

Speirs, Z.C., Loynes, C.A., Mathiessen, H., Elks, P.M., Renshaw, S.A., and Jørgensen, L.v.G., 2024. What can we learn about fish neutrophil and macrophage response to immune challenge from studies in zebrafish. Fish & Shellfish Immunology 148: 109490. http://doi.org/10.1016/j.fsi.2024.109490

Tian, J., Zeng, X.B., Zhang, S., Wang, Y.Z., Zhang, P., Lü, A.J., and Peng, X., 2014. Regional variation in components and antioxidant and antifungal activities of *Perilla frutescens* essential oils in China. Industrial Crops and Products 59: 69–79. http://doi.org/10.1016/j.indcrop.2014.04.048

Wang, J., 2018. Neutrophils in tissue injury and repair. Cell and Tissue Research 371(3): 531–539. http://doi.org/10.1007/s00441-017-2785-7

Wang, X.-F., Li, H., Jiang, K., Wang, Q.-Q., Zheng, Y.-H., Tang, W., and Tan, C.-H., 2018. Anti-inflammatory constituents from Perilla frutescens on lipopolysaccharide-stimulated RAW264.7 cells. Fitoterapia 130: 61–65. http://doi.org/10.1016/j.fitote.2018.08.006

Wang, S.-q., Xiang, J., Zhang, G.-q., Fu, L.-y., Xu, Y.-n., Chen, Y., Tao, L., Hu, X.-x., and Shen, X.-c., 2024. Essential oil from Fructus Alpinia zerumbet ameliorates atherosclerosis by activating PPARγ-LXRα-ABCA1/G1 signaling pathway. Phytomedicine 123: 155227. http://doi.org/10.1016/j.phymed.2023.155227

Wang, L.L., Yu, M.J., Ding, S.W., Cao, J.Z., Meng, X.H., Li, L., Sa, R., He, M., and Sun, M.M., 2023. Zebrafish models for the evaluation of essential oils (EOs): A comprehensive review. Quality Assurance and Safety of Crops & Foods 15(4): 156–178. http://doi.org/10.15586/qas.v15i4.1384

Wu, H., Denna, T.H., Storkersen, J.N., and Gerriets, V.A., 2019. Beyond a neurotransmitter: The role of serotonin in inflammation and immunity. Pharmacological Research 140: 100–114. http://doi.org/10.1016/j.phrs.2018.06.015

Wu, X., Dong, S., Chen, H., Guo, M., Sun, Z., and Luo, H., 2023. Perilla frutescens: A traditional medicine and food homologous plant. Chinese Herbal Medicines (CHM) 15(3): 369–375. http://doi.org/10.1016/j.chmed.2023.03.002

Yu, H., Qiu, J.F., Ma, L.J., Hu, Y.J., Li, P., and Wan, J.B., 2017. Phytochemical and phytopharmacological review of *Perilla frutescens* L. (Labiatae), a traditional edible-medicinal herb in China. Food and Chemical Toxicology (FCT) 108: 375–391. http://doi.org/10.1016/j.fct.2016.11.023

Zaccherini, G., Aguilar, F., Caraceni, P., Clària, J., Lozano, J.J., Fenaille, F., Castelli, F., Junot, C., Curto, A., Formentin, C., Weiss, E., Bernardi, M., Jalan, R., Angeli, P., Moreau, R., and Arroyo, V., 2021. Assessing the role of amino acids in systemic inflammation and organ failure in patients with ACLF. Journal of Hepatology 74(5): 1117–1131. http://doi.org/10.1016/j.jhep.2020.11.035

Zanandrea, R., Bonan, C.D., and Campos, M.M., 2020. Zebrafish as a model for inflammation and drug discovery. Drug Discovery Today 25(12): 2201–2211. http://doi.org/10.1016/j.drudis.2020.09.036

Zhang, Y.R., Liu, Y.R., Tang, Z.S., Song, Z.X., Zhang, J.W., Chang, B.J., Zhao, M.L., and Xu, J., 2022. *Rheum officinale* Baill. Treats zebrafish embryo thrombosis by regulating NOS3 expression in the arginine biosynthesis pathway. Phytomedicine 99: 13. http://doi.org/10.1016/j.phymed.2022.153967

Zheng, P., 2009. Neuroactive steroid regulation of neurotransmitter release in the CNS: Action, mechanism and possible significance. Progress in Neurobiology 89(2): 134–152. http://doi.org/10.1016/j.pneurobio.2009.07.001

Zhong, Y., Du, Q., Wang, Z.Q., Zheng, Q., Yang, M., Hu, P.Y., Yang, Q.Y., Xu, H.H., Wu, Z.F., Huang, X.Y., Li, H.T., Tang, M.X., Zeng, H.M., Zhu, L.Y., Ren, G.L., Cao, M., Liu, Y., and Wang, H.B., 2024. Antidepressant effect of *Perilla frutescens* essential oil through monoamine neurotransmitters and BDNF/TrkB signal pathway. Journal of Ethnopharmacology 318: 10. http://doi.org/10.1016/j.jep.2023.116840

Zhou, P.N., Yin, M.J., Dai, S.L., Bao, K., Song, C.L., Liu, C.C., and Wu, Q.A., 2021. Multi-omics analysis of the bioactive constituents biosynthesis of glandular trichome in *Perilla frutescens*. Bmc Plant Biology 21(1): 15. http://doi.org/10.1186/s12870-021-03069-4

Zi, Y.X., Yao, M.J., Lu, Z.X., Lu, F.X., Bie, X.M., Zhang, C., and Zhao, H.Z., 2021. Glycoglycerolipids from the leaves of *Perilla frutescens* (L.) Britton (Labiatae) and their anti-inflammatory activities in lipopolysaccharide-stimulated RAW264.7 cells. Phytochemistry 184: 9. http://doi.org/10.1016/j.phytochem.2021.112679

Appendix

GC-MS detection conditions: For gas chromatography (GC), the initial oven temperature was set to 45°C and held for 2 min. Next, the temperature was gradually increased to 280°C at a rate of 5°C per minute, and was maintained at 280°C for additional 10 min. Helium carrier gas flowed through the system at a linear velocity of 2.2 mL/min. For mass spectrometry, the mass-to-charge range was set to 40–500 m/z, and the ion source temperature to 230°C.

2. RNA sequencing (RNA-Seq) assay detection conditions: After treatment using the same method as described above, 10 whole zebrafish larvae were collected in a 1.5-mL centrifuge tube; each group had three tubes. Water was removed and each tube was put into liquid nitrogen and transferred to -80°C refrigerator. Total RNA was isolated from larval zebrafish with Trizol reagent (Thermo Fisher Scientific). NanoDrop 2000 (Thermo Fisher Scientific) and Bioanalyzer 2100 system (Agilent Technologies Inc.) were performed to assess the concentration and integrity of isolated RNA, respectively. After adding fragmentation buffer, mRNA was fragmented and cDNA was synthesized under the guidelines from Illumina (USA). Next, for qualified libraries, PCR was used to construct final cDNA libraries, and paired-end technology was used for next-generation sequencing (NGS) using Illumina sequencer with a read length of 2×150 base pairs long (bp). Each group contained three biological replicates.

3. Metabolomics detection conditions: In each group, 10 whole zebrafish larvae were collected and pooled followed by quick-freezing in liquid nitrogen. The zebrafish larvae were homogenized with a homogenizer after adding 400-μL methanol and 125-μL water. The samples were subjected to vortex for 1 min and shaking for 5 min at room temperature after addition of 400-μL chloroform and 200-μL water. Samples were centrifuged at 12,000 revolutions per minute (rpm) for 10 min at 4°C, and the supernatant was used for metabolomics analysis. Each group contained three biological replicates.

Subsequently, Agilent 1290 Infinity ultra performance liquid chromatography (UPLC; Agilent Technologies Inc.) and Agilent 6540 UHD Accurate-Mass Q-TOF mass spectrometer (Agilent Technologies Inc.) were used to separate and identify the extracts, respectively. Acquity UPLC HSS T3 column (2.1×100 mm, 1.8 μm; Waters, USA) was equipped with UPLC whereas an electrospray ionization interface was equipped with mass spectrometry. Detection conditions were as follows: for UPLC, the column oven was maintained at 40°C with 0.3-mL/min flow rate, and injection 2 μL into column. The mobile phase consisted of (A) acetonitrile and (B) 0.2% formic acid in water, which were applied for the following gradient elution program: 95–80% A, 0–2 min; 80–40% A, 2–5 min; 40–1% A, 5–6 min; 1% A, 6–7.5 min; 1–95% A, 7.5–7.6 min; and 95% A, 7.6–10 min. For mass spectrometry, the mass-to-charge range was set to 50–1,000 m/z, scanned at 2 spectra/s. Desolvation was done with nitrogen at 320°C at a flow of 10 L/min.

Table A1. Additional details about RT-PCR.

Gene	Product length (bp)	Annealing temperature	References
β-*actin*	110	60°C	(Hedrera *et al.*, 2013)
TNF-α	182	60°C	(He *et al.*, 2020)
IL-6	119	60°C	(He *et al.*, 2020)
*IL-1*β	150	60°C	(Hedrera *et al.*, 2013)
glula	197	60°C	(Gong *et al.*, 2020)
pyya	291	60°C	(Gong *et al.*, 2020)

pyya: peptide YYa;